Properties of hot subdwarfs in the *GALEX* survey

Péter Németh, Stéphane Vennes & Adéla Kawka

Astronomický ústav AV ČR, CZ-251 65 Ondřejov, Czech Republic
nemeth,vennes,kawka@sunstel.asu.cas.cz

Abstract: We have analyzed a sample of hot subdwarfs (sdB, sdO) selected from the *GALEX* ultraviolet sky survey. Applying a model atmosphere analysis we determined the temperature, surface gravity, and helium-to-hydrogen abundance ratio, and obtained preliminary constraints on the CNO abundance for a sample of ∼200 stars. Adopting colourimetric (ultraviolet-infrared) and spectroscopic criteria (Mg I, Ca II, etc.) we also investigated the incidence of solar type or earlier companions. We present the results of our analysis and discuss some of the challenges encountered.

Introduction

A quest for new, bright white dwarf and hot subdwarf stars was initiated by Vennes et al. (2011): The targets were selected based on colour criteria using *GALEX* $N_{\rm UV}$, GSC V and 2MASS J and H magnitudes. This process provided ∼700 sources with $N_{\rm UV}-V<0.5$. Many of these turned out to be previously unknown subdwarf stars requiring new observations. To maximize the white dwarf sample, our spectroscopic follow-up was carried out in the order of decreasing reduced proper-motion index. Here we report part of our results on 181 hot subdwarf stars. A similar catalogue of hot subdwarf stars was built by Oreiro et al. (2011) using ultraviolet/optical/infrared colours. Sample of bright subdwarf B stars are useful in identifying candidates for pulsation studies (e.g., Østensen et al., 2010) or radial velocity studies (e.g., Geier et al., 2011).

Observations

Low-dispersion optical spectra were obtained at two sites during five observing runs between 2008 and 2011. At ESO, we used the EFOSC2 spectrograph attached to the 3.6m NTT telescope with grisms #11 (300 lines/mm) and #7 (600 lines/mm) resulting in resolutions of $\Delta\lambda\sim13.7$ and ~6.4 Å, respectively. At KPNO, we used the RC spectrograph attached to the 4m Mayall telescope with the KPC-10A (316 lines/mm) grating delivering a spectral resolution of $\Delta\lambda\sim5$ Å. The KPNO spectra and the low-resolution ESO data covers the entire Balmer line series from 3700 to 7400 Å. The ESO $\Delta\lambda\sim6.4$ Å resolution data spans from 3600 to 5200 Å covering the upper Balmer line series. All data were reduced using standard IRAF procedures.

Spectral fitting

The non-LTE model atmosphere codes TLUSTY and SYNSPEC (Hubeny & Lanz 1995 and Lanz & Hubeny 1995) were used for our spectral diagnostics. TLUSTY calculates plane–parallel, horizontally homogeneous stellar atmospheres in radiative and hydrostatic equilibrium treating metal line blanketing by means of opacity sampling. Model atoms were taken from the OSTAR and BSTAR database. The most detailed model atoms were included for He I - II, C II-IV, N III - V and O IV - VI giving altogether 350 energy levels and about 5800 explicit transitions.

Our χ^2 minimization method is based on a combination of the steepest-descent and simplex algorithms. Starting out from an initial model, all parameters are varied in the maximal range that TLUSTY convergence allows for. To approach the global minimum, step sizes are adjusted as necessary for all parameters independently. Information from previous iterations is used to accelerate the procedure, and slow evolving parameters can be relaxed. The χ^2 is calculated for the entire spectrum, normalized to the continuum in appropriately sized segments to account for the broad H and He, and narrow metal lines. Fitting is continued until maximum relative changes of the model parameters and χ^2 are all below 0.5% in three consecutive iterations. Errors are estimated by mapping the χ^2 around final parameters (X) at representative points in the range of $\log(\delta X/X)<\pm2$.

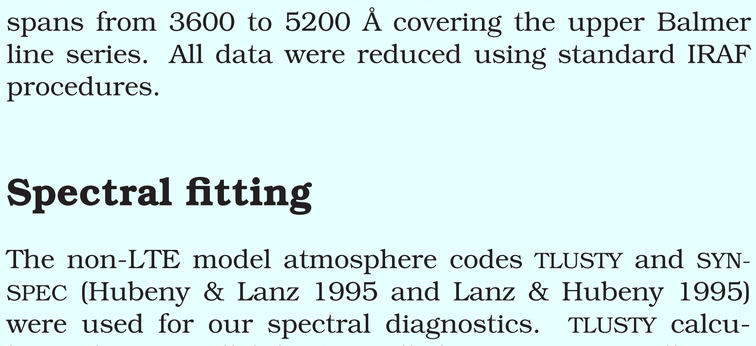

Figure 1: Observed NTT and best fitting model spectrum for GALEXJ2059–4232. Identifications are given for He, CNO lines with equivalent widths larger than 1 Å.

Starting out from a model at $T_{\rm eff}=40000$ K, $\log g=5.6$ cm/s^2, $\log n({\rm He})/n({\rm H})=-1$ and $\log n({\rm CNO})/n({\rm H})=-2$, we could carry out model atmosphere analyses for ∼200 stars in ∼800 hours by distributing the calculations on six processors. Figure 1 shows our fit of the He-sdB star GALEX J2059–4232. Table 1 lists a subset of our results.

Table 1: Properties of hot subdwarf stars. Three out of the first ten stars are in double-lined binaries. Binary mass-ratio ($q_{\rm bb}$) is derived from black-body spectral distribution using the best fitting model parameters.

GALEXJ	Type	V	$T_{\rm eff}$	$\log g$	Abundances, $\log n({\rm X})/n({\rm H})$				V − J	J − H	Comments
		(mag)	(K)	(cm/s^2)	He	C	N	O	(mag)	(mag)	
0035+2459	sdB	14.16	35230^{+740}_{-700}	$5.66^{+0.07}_{-0.15}$	$-2.91>$	$-4.94>$	$-4.45>$	$-4.19>$	−0.474	−0.152	
0036+3755	sdB	14.07	38970^{+500}_{-1330}	$5.89^{+0.10}_{-0.09}$	$-3.20>$	$-5.10>$	$-4.00>$	$-4.79>$	−0.709	−0.097	
0047+0337*a*	sdB	12.39	38620^{+2250}_{-970}	$6.14^{+0.22}_{-0.18}$	$-2.63^{+0.44}_{-1.17}$	$-4.69>$	$-3.61>$	$-4.13>$	0.510	0.251	$f_{5200}=0.459$, $q_{\rm bb}=0.95$
0047+0337*b*	F6V		6140	4.14							[Fe/H] = −0.55
0049+2056	sdB	14.72	27520^{+500}_{-450}	$5.55^{+0.07}_{-0.06}$	$-2.48^{+0.16}_{-0.23}$	$-4.16>$	$-4.05^{+0.35}_{-0.58}$	$-4.11>$	−0.371	−0.062	
0111+1947	sdB	14.46	42780^{+540}_{-820}	$5.87^{+0.09}_{-0.07}$	$-2.27^{+0.17}_{-0.17}$	$-4.77>$	$-3.51>$	$-4.28>$	−0.846	−0.193	
0115+1922*a*	sdB	13.09	31060^{+680}_{-650}	$6.12^{+0.20}_{-0.16}$	$-2.57>$	$-4.02>$	$-3.68>$	$-3.48>$	0.428	0.086	$f_{5200}=0.363$, $q_{\rm bb}=0.72$
0115+1922*b*	F2V		6710	4.38							[Fe/H] = −0.39
0115+2614	sdO	14.51	55470^{+1840}_{-1620}	$5.66^{+0.40}_{-0.10}$	$0.03^{+1.06}_{-0.05}$	$-3.75^{+0.89}_{-1.02}$	$-3.42^{+0.63}_{-0.42}$	$-2.96>$	−0.468	−0.082	
0116+0603*a*	sdB	13.24	35310^{+620}_{-380}	$6.08^{+0.24}_{-0.05}$	$-1.70^{+0.13}_{-0.13}$	$-3.55>$	$-4.80^{+1.18}_{-0.66}$	$-3.74>$	0.926	0.169	$f_{5200}=0.368$, $q_{\rm bb}=0.74$
0116+0603*b*	F6V		6170	4.09							[Fe/H] = −0.15
0119+4901	sdO	13.56	43730^{+280}_{-620}	$5.84^{+0.07}_{-0.14}$	$0.17^{+0.38}_{-0.05}$	$-2.76>$	$-2.70^{+0.82}_{-0.11}$	$-3.02^{+0.46}_{-1.02}$	−0.244	−0.257	
0154+4905	sdB	13.51	32100^{+410}_{-240}	$5.50^{+0.32}_{-0.02}$	$-1.98^{+0.15}_{-0.08}$	$-4.67>$	$-4.20>$	$-4.86>$	−0.332	0.096	
⋮						⋮					⋮

Binary decomposition

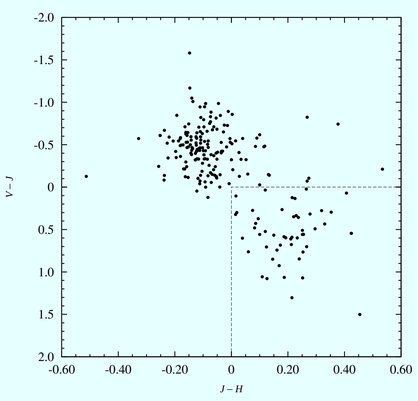

Figure 2: $V-J$ vs. $J-H$ colour–colour diagram for our subdwarf sample. Optical magnitudes were collected from GSC 2.3.2 and infrared form the 2MASS database using VizieR. Apparently single stars aggregate near $V-J\approx-0.5$ and $J-H\approx-0.1$, while composite-spectra binaries show infrared excess (lower right corner).

Binarity plays an important role in the theory of subdwarf formation and evolution. Indeed, a large fraction of subdwarfs are found in binary systems: ∼20% show composite spectra while ∼30% are in close binaries (Heber, 2009). In our sample, about 15% shows strong double lined composite spectra in accordance with Figure 2, where 19% of the stars have $V-J>0$ and $J-H>0$. Moreover, 25% of our sample shows noticeable CaII, MgI or Fe G band absorption.

Two of these stars turned out to be in close binaries based on radial velocity studies (Kawka et al., 2010). Further spectroscopic and photometric follow-up observation are necessary to find more of these binaries.

In double-lined binaries both components can be examined simultaneously. Figure 3 shows an example of spectroscopic decomposition. We built a library of template spectra from the MILES (Cenarro et al., 2007) database to characterize the cool component. This semi-empirical approach is considered less ambiguous than working with synthetic spectra for both components. The best fitting secondary spectrum was searched by interpolating in temperature, surface gravity and metallicity [Fe/H] along with TLUSTY model parameters for the primary. In the first step only spectral lines were considered to select an approximate template spectrum. From the second iteration both the spectral template and the flux ratio of the components were updated.

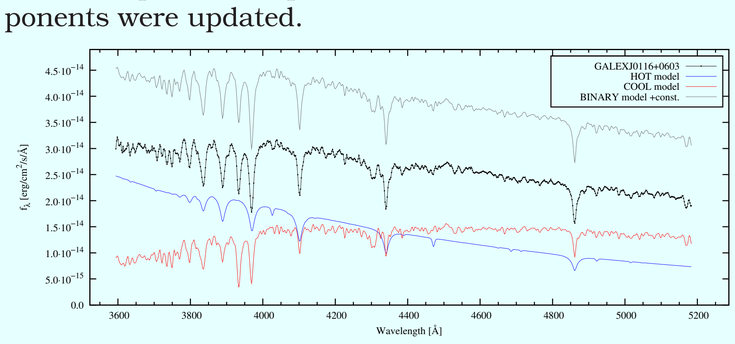

Figure 3: Spectral decomposition of GALEXJ0116+0603.

Our method worked well for binaries with late type (F,G,K) companions where components have distinct spectral features. However, due to spectral similarities of hot subdwarf and early type stars, it is less sensitive for A type companions, although population syntheses (Han et al., 2003) predict these. Higher resolution spectra, complemented with radial velocity and photometric analysis can help resolving such binaries.

Subdwarf atmospheric properties

Figure 4 shows the distribution of analysed hot subdwarfs in the $T_{\rm eff}-\log g$ plane, while Figure 5 shows the measured He abundance as a function of effective temperature.

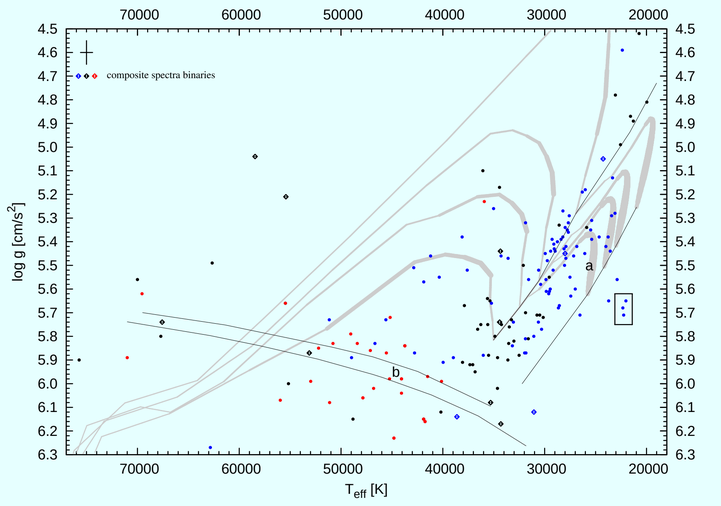

Figure 4: $T_{\rm eff}-\log g$ diagram. Most stars reside near the EHB (a), and the helium main sequence (b). The grey lines are theoretical evolutionary tracks from Dorman et al. (1993) for stellar masses from top to bottom: 0.480, 0.475, 0.473 and 0.471 $M_\odot$. Line widths are proportional to evolutionary time scales. Typical error bars are shown in the upper left corner. Data points in the rectangle at $T_{\rm eff}=22100$ K and $\log g=5.68$ (cgs) are three independent observations of the same star. He rich ($\log n({\rm He})/n({\rm H})>0$) stars are indicated in red, He poor ($\log n({\rm He})/n({\rm H})<-2$) stars in blue and stars with $-2<\log n({\rm He})/n({\rm H})<0$ are in black. Subdwarfs in resolved composite spectra binaries are shown with diamonds.

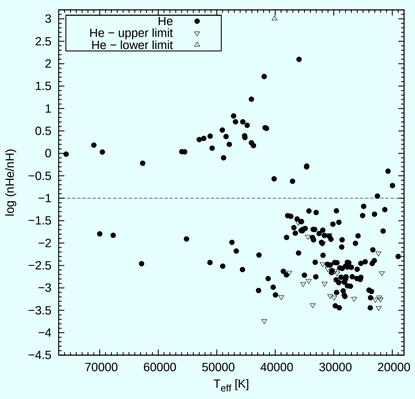

Figure 5: He abundance vs. effective temperature. Regions for sdBs, He-sdBs and helium rich sdOs can be distinguished. A trend of increasing He abundance with effective temperature can be outlined.

References

Cenarro A. J., Peletier R. F., Sánchez-Blázquez P., Selam S. O., Toloba E., Cardiel N., Falcón-Barroso J., Gorgas J., Jiménez-Vicente J., Vazdekis A., 2007, MNRAS, 374, 664
Dorman B., Rood R. T., O'Connell R. W., 1993, ApJ, 419, 596
Geier S., Hirsch H., Tillich A., Maxted P. F. L., Bentley S. J., Østensen R. H., Heber, U., Gänsicke B. T., Marsh T. R., Napiwotzki, R., Barlow B. N., O'Toole S. J., 2011, A&A, 530, A28
Han Z., Podsiadlowski Ph., Maxted P. F. L., Marsh T. R., Ivanova N., 2003, MNRAS, 336, 449
Heber U., 2009, Annu. Rev. A&A, 47, 211
Hubeny I., Lanz T., 1995, ApJ, 439, 875
Kawka A., Vennes S., Nemeth P., Kraus M., Kubát J., 2010, MNRAS, 408, 992
Lanz T., Hubeny I., 1995, ApJ, 439, 905
Oreiro R., Rodríguez-López C., Solano E. Ulla A., Østensen R., García-Torres, M., 2011, A&A, 530, A2
Østensen R. H., Oreiro R., Solheim J.-E., Heber U., Silvotti R., González-Pérez J. M., Ulla A., Pérez Hernández F., Rodríguez-López,, C. Telting J. H., 2010, A&A, 513, A6
Vennes S., Kawka A., Nemeth P., 2011, MNRAS, 410, 2095